

# Structural, Electronic and Thermochemical Characterizing the Graphene Doped with Transition Metals for Nitrogen Dioxide Adsorption: A Gas Sensing Study by Ab Initio Method

Fatemeh Mollaamin<sup>1,2\*</sup>, Sara Shahriari<sup>3</sup>, Karim Zare<sup>4</sup>

<sup>1</sup> Department of Food Engineering, Faculty of Engineering and Architecture, Kastamonu University, Kastamonu, Turkey

<sup>2</sup> Department of Biology, Faculty of Science, Kastamonu University, Kastamonu, Turkey

<sup>3</sup> Department of Chemistry, Central Tehran Branch, Islamic Azad University, Tehran, Iran

<sup>4</sup> Department of Chemistry, Science and Research Branch, Islamic Azad University, Tehran, Iran

\* Correspondence: smollaamin@gmail.com (F.M.);

Scopus Author ID 35848813100

Received: 13.03.2023; Accepted: 28.05.2023; Published: 4.02.2024

**Abstract:** In this research, nitrogen dioxide (NO<sub>2</sub>) adsorption on doped pristine graphene (Gr) sheets with transition metals (TM) of manganese (Mn), cobalt (Co), and copper (Cu) has been applied for scavenging this toxic gas as the environmental pollutant. TM@GR yields higher activity toward gas sensing than pure graphene. The thermodynamic results from IR spectroscopy have indicated that  $\Delta G_{\text{ads,NO}_2 \rightarrow \text{TM@C-NG}}^{\circ}$  values are similar for different metal transitions of Mn, Co, Cu, which exhibit the accord of the estimated data by all approaches. Our results have provided a favorable understanding of the interaction between TM-doped graphene nanosheet and NO<sub>2</sub> gas molecule. The bonding of NO<sub>2</sub> molecule to transition metals of Mn, Co, and Cu can be observed as beginning by transferring the unpaired electron into empty d orbitals of transition metal atoms. Moreover, NQR method with EPR-III basis set for N-atoms has approved the efficiency of nitrogen dioxide as the detectors for promising scavengers through the graph analysis of  $:\ddot{\text{O}}: -\dot{\text{N}} = \ddot{\text{O}}: \rightarrow \text{Mn@C-Gr}$ ,  $:\ddot{\text{O}}: -\dot{\text{N}} = \ddot{\text{O}}: \rightarrow \text{Co@C-Gr}$ ,  $:\ddot{\text{O}}: -\dot{\text{N}} = \ddot{\text{O}}: \rightarrow \text{Cu@C-Gr}$  complexes. Furthermore, the results of partial electron density states (PDOS) have confirmed an obvious charge accumulation between the graphene and doped atoms Mn, Co, Cu through NO<sub>2</sub> adsorption. Frontier molecular orbital's of HOMO, LUMO, and band energy gap accompanying some chemical reactivity parameters have represented the attributes of molecular electrical transport of (Mn, Co, Cu) doping of carbon nanographene for NO<sub>2</sub> adsorption.

**Keywords:** NO<sub>2</sub>; Gas sensor; (Mn, Co, Cu) @Gr; nanographene sheet; environmental pollutant; ONIOM/CAM; Langmuir adsorption.

© 2024 by the authors. This article is an open-access article distributed under the terms and conditions of the Creative Commons Attribution (CC BY) license (<https://creativecommons.org/licenses/by/4.0/>).

## 1. Introduction

Sensing and grabbing toxic and harmful gases like CO, CO<sub>2</sub>, NO, N<sub>2</sub>O, CH<sub>4</sub>, SO<sub>2</sub>, and H<sub>2</sub>S can largely help maintain human health and the ecosystem [1-5]. Different usages of carbon nanocompounds, such as adsorbing hydrogen, hazardous compounds, and gas and designing the sensor instruments [6-10]. Recently, many materials, including carbon structures, have been designed and applied for the adsorptive removal of environmental pollutant gases [11-15]. Thus, making high-implement gas detectors to distinguish these compounds is essential.

Therefore, the remarkable surface of carbon nanostructures is a privileged factor for gas detecting and adsorbing gas devices [16-19]. In addition, enough implanting of the compounds with transition metals might enhance their adsorbing ability and adjust their adsorbing selectivity as excellent dopant applicants [20-23].

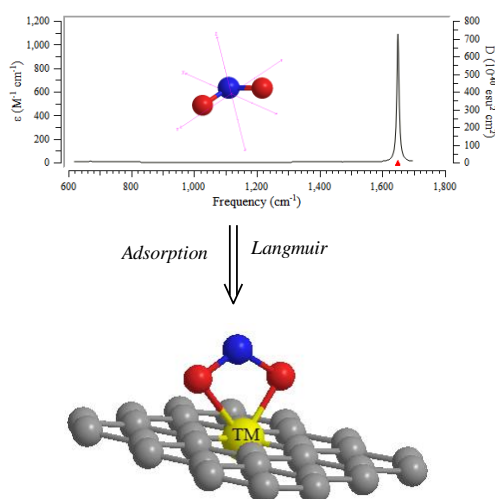
As a matter of fact, this research wants to investigate the adsorption of hazardous gas of NO<sub>2</sub> on the carbon nanographene, which has been decorated by transition metals of manganese, cobalt, and copper using DFT (density functional theory) approach to discover the adsorbing parameters of the various TM-doped nanographene surfaces [24-29].

## 2. Materials and Methods

This article discusses the adsorbing of NO<sub>2</sub> onto the transition metals-doped carbon nanographene. It has been defined as the first process of bond formation arising in the meanwhile of NO<sub>2</sub> chemisorption. It runs over the consequences gained for adsorbing NO<sub>2</sub> onto (Mn, Co, Cu) doping of carbon nanographene. Bonding of NO<sub>2</sub> molecule to a TM atom on the Gr surface can be observed as first launching by giving the lone pair on the C-atom into unoccupied d orbitals of the TM atom. The donor potency of NO<sub>2</sub> in this procedure is recognized to be much tiny, and stability of the TM-C bond is confirmed to be captured by back donation of electrons from occupied d orbitals on the metal into unoccupied antibonding  $\pi^*$  orbitals on the NO<sub>2</sub> gas molecules. It is assumed that the two steps, donation and back donation, intend to augment each other in a cooperative state [30,31].

Different studies have concentrated on the C- nanosurfaces' gas adsorbing susceptibilities, which denote a good accord with the Langmuir adsorbing template. The adsorption of toxic NO<sub>2</sub> gas on the Mn-doped, Co-doped, Cu -doped graphene nanosheet has been approved by the most appropriate Langmuir isotherm, which indicates the nature of chemisorption for the bond distance between : $\ddot{O}$ : - $\dot{N}$  =  $\ddot{O}$ : molecules and TM-doped C-nanographene, the equilibrium electron diffusion of the adsorbed particles between the solid and gas phases, and a monolayer feature. The gas molecules of : $\ddot{O}$ : - $\dot{N}$  =  $\ddot{O}$ : are kept on TM-doped C-nanographene with Langmuir chemisorption (Scheme 1).

The changes of charge density analysis in the adsorption process have illustrated that Mn-doped, Co-doped, Cu -doped C-nanographene show the Bader charge of -1.499,-2.241,-1.570, respectively, before adsorption of NO<sub>2</sub>, and -1.549,-1.794, -1.708, respectively, after adsorption of NO<sub>2</sub> (Figure 1).



**Scheme 1.** IR spectrums of : $\ddot{O}$ : - $\dot{N}$  =  $\ddot{O}$ : molecules that adsorb on (Mn, Co, Cu) doping of C-nanographene.

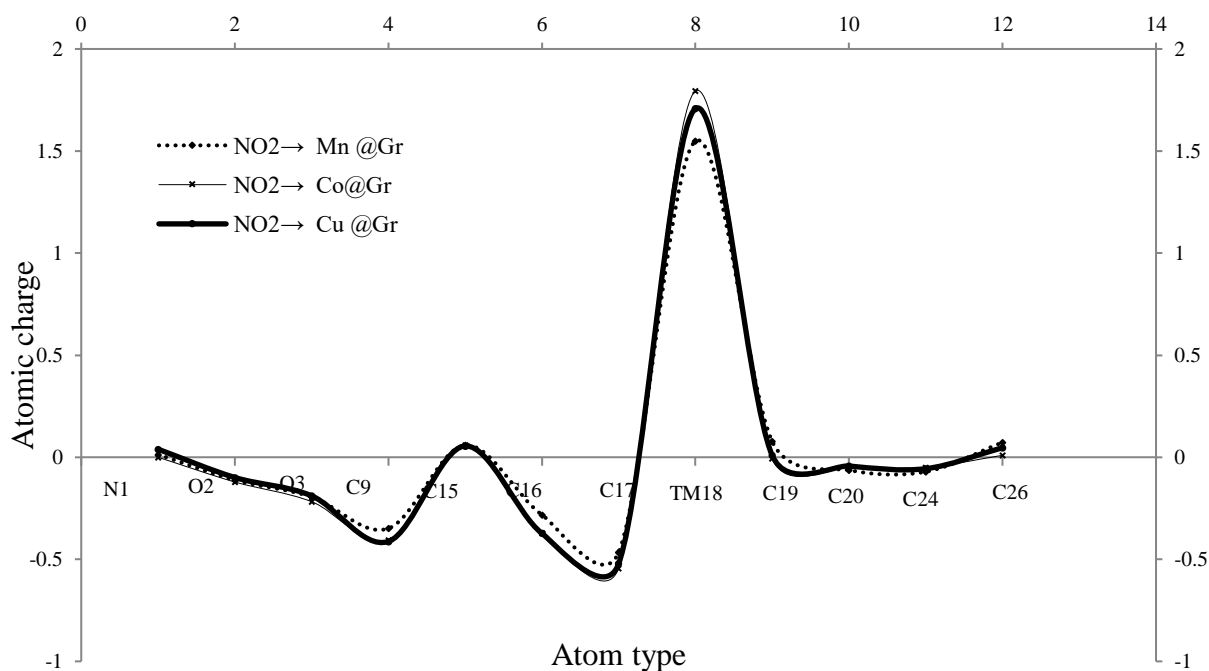
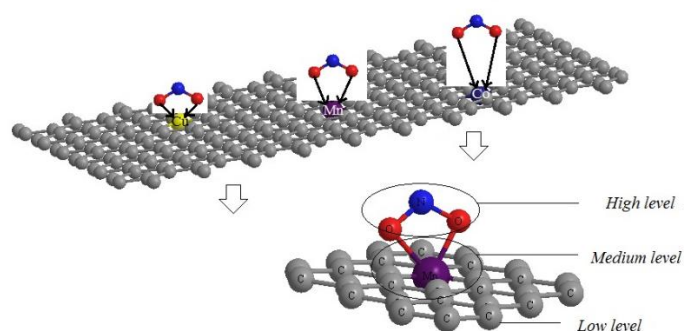


**Figure 1.** The fluctuation of charge distribution versus atom type for adsorbing NO<sub>2</sub> on the (Mn, Co, Cu) @Gr.

Therefore, the changes of charge density for Langmuir adsorption of nitrogen dioxide on Mn-doped, Co-doped, and Cu-doped C-nanographene alternatively are  $\Delta Q_{Cu-doped} = -0.138 > \Delta Q_{Mn-doped} = -0.05 \gg \Delta Q_{Co-doped} = +0.447$ . The values of charge density changes have illustrated a more significant charge transfer for Cu-doped C-nanographene (Figure 1).

Our own n-layered integrated molecular orbital and molecular mechanics, or ONIOM combines three theoretical levels to reduce the sequence of validity as the high, medium, and low degrees of theory. In this model, a high-degree level has been performed using the density functional theory insight of CAM-B3LYP wave function with 6-31+G (d, p) basis set for some carbon atoms in nanographene and oxygen atoms in the adsorption zone; EPR-III basis set for nitrogen and LANL2DZ for some manganese, cobalt, copper atoms through adsorbing NO<sub>2</sub> in the adsorption zone. The medium-degree level has been considered on the other carbon atoms of nanographene in the adsorption zone owing to semi-empirical methodologies. At last, a low-degree level has been depicted on the other manganese, cobalt, and copper atoms through the adsorption of NO<sub>2</sub> with MM2 force fields of molecular mechanic methods as formula (Scheme2) [32-34]:

$$E_{ONIOM} = E_{High} + E_{Medium} + E_{Low} \quad (1)$$



**Scheme 2.** Langmuir adsorbing of NO<sub>2</sub> as the pollutant toxic gas onto (Mn, Co, Cu) doping of C-nanographene graphene on the optimized structure due to three-degree layered of high, medium, and low levels of ONIOM model.

In other words, the three-degree model of ONIOM leads to exploring a ground order more precisely than the one-degree model, which might treat a medium-sized order exactly such as a huge order with admissible validity [35].

In this article, the structures have been computed using the CAM-DFT method on the adsorption mechanisms of NO<sub>2</sub> by (Mn, Co, Cu) doping of C-nanographene through bonding between transition metals and gas molecules. It has been discovered that the surface binding zone preference of O-atom and N-atom of NO<sub>2</sub> in the adsorption zone is greatly influenced by the existence of neighboring atoms in the C-nanographene. The calculated pair distribution functions in NO<sub>2</sub>→ Mn/Co/Cu doping of C-NG have depicted that the creation of complexes leads to shorter bond lengths of O→ Mn, O→ Co, and O→ Cu, respectively, once balanced to the analogous increment (Scheme 2).

Concerning DFT or Density Functional Theory, hybrid functional is considered a series of approximations for the exchange-correlation energy functional, which merges a sector of precise exchange from HF or Hartree-Fock theory methodology with the remainder of the exchange-correlation energy from other notifications like empirical or ab initio approaches. Thus, the Kohn-Sham orbitals represent the precise exchange energy functional instead of density, which is located as the indirect density functional. This research has employed the impression of the hybrid functional of a three-parameter basis set of Becke, Lee, Yang, Parr (B3LYP) within the skeleton of DFT upon theoretical computations [36,37].

A transition metal-doped graphene sheet has been made using the hard system and Z-Matrix format, in which a blank line has been positioned. The hard Potential Energy Surface has been exposed at CAM-B3LYP functional [38], and concerning LANL2DZ /6-31+ G (d,p) basis sets to appoint frontier molecular orbital, Mulliken charges, nuclear magnetic resonance properties, dipole moment, thermodynamic characteristics and other quantum attributes [39]. In this research, NO<sub>2</sub> has been adsorbed onto TM-doped C-nanographene toward the formation of NO<sub>2</sub>→ Mn/Co/Cu doping of C-Gr sheet using the Gaussian 16 program package [40].

### 3. Results and Discussion

Based on the computational results, manganese, iron, cobalt, nickel, copper, and zinc transition metals doped on the nanographene have been investigated as the efficient surface for adsorption of toxic gas of nitrogen dioxide (NO<sub>2</sub>) causing air pollution. These experiments have been accomplished using spectroscopy analysis through some physicochemical attributes.

#### 3.1. Electronic properties (DOS & PDOS).

The electronic structures of : $\ddot{O}$ : - $\dot{N}$  =  $\ddot{O}$ : → Mn@ C-Gr, : $\ddot{O}$ : - $\dot{N}$  =  $\ddot{O}$ : →Co @C-Gr, : $\ddot{O}$ : - $\dot{N}$  =  $\ddot{O}$ : → Cu @C-Gr complexes have been analyzed to simplify subsequent discussion for interfacial electronic properties using DFT/LANL2DZ basis set. The graph of partial DOS (PDOS) has illustrated that the p states of Mn/Co/Cu-doped in the nanographene surface are dominant through the conduction band (Figure 2a-c). A distinct metallic feature can be observed in the TM@C-Gr surface because of the strong interaction between the p states of C-Gr and the d state of Mn, Co, and Cu atoms near the Fermi energy. Moreover, the existence of covalent features for these alloys has exhibited identical energy amounts and figures of the PDOS for the p orbitals of C-Gr and d orbitals of Mn, Co, and Cu atoms.

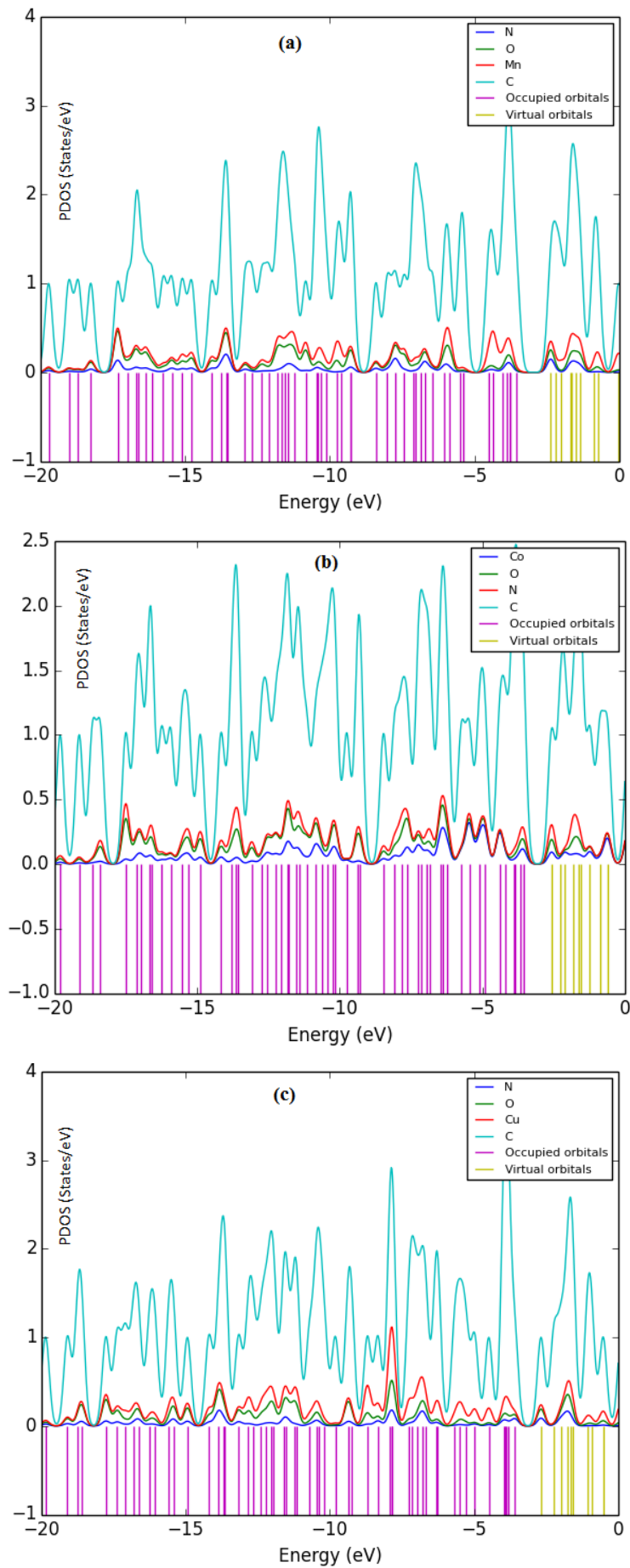


**Figure 2.** PDOS of (a)  $\text{NO}_2 \rightarrow \text{Mn@C-Gr}$ , (b)  $\text{NO}_2 \rightarrow \text{Co@C-Gr}$ , and (c)  $\text{NO}_2 \rightarrow \text{Cu@C-Gr}$  with Fermi level = 0.

Figure 2(a-c) shows that the Mn, Co, and Cu states doped in the graphene surface contribute more at the middle of the conduction band between -1ev and -20ev. The contribution of C, N, O, Mn, Co, Cu states are expanded, but C states in the graphene nanosheet reveal the expanded contribution with sharper conduction bands compared to N, O, Mn, Co, Cu states (Figure 2a-c).

The partial electron density (PDOS) also approved the results, showing a charge association between the graphene sheet and Mn, Co, and Cu-doped elements. Thus, the above results exhibit that the cluster dominant of non-metallic and metallic features and a certain degree of covalent features can illustrate the increasing adsorption direct band gap of NO<sub>2</sub> through (Mn, Co, Cu)-doped graphene nanosheet.

### 3.2. Nuclear quadrupole resonance (NQR) analysis.

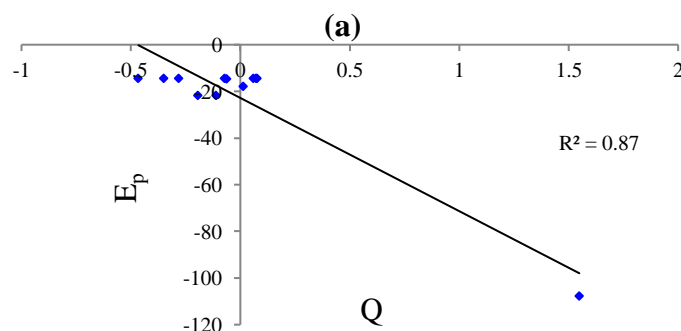
NQR method has been carried out for the complexes of NO<sub>2</sub> adsorption on the (Mn, Co, Cu) -doped carbon nanographene [41-44].

As the EFG at the position of the nucleus in gas adsorbed on the metal-doped carbon nanographene as the gas sensor is assigned by the valence electrons twisted in the special linkage with close nuclei of C-nanographene surface, the NQR frequency at which transitions happen in particular for : $\ddot{O}$ : - $\dot{N}$  =  $\ddot{O}$ :  $\rightarrow$  (Mn, Co, Cu)- doped C-nanographene (Table1).

**Table 1.** The electric potential( $E_p$ ) and Bader charge (Q) for elements of NO<sub>2</sub> $\rightarrow$  Mn-doped, NO<sub>2</sub> $\rightarrow$  Co-doped, NO<sub>2</sub> $\rightarrow$  Cu-doped nanographene by CAM-B3LYP/EPR-III, LANL2DZ,6-31+G(d,p) calculation extracted of NQR method.

: $\ddot{O}$ : - $\dot{N}$ = $\ddot{O}$ : $\rightarrow$ Mn@ C-NG			: $\ddot{O}$ : - $\dot{N}$ = $\ddot{O}$ : $\rightarrow$ Co@ C-NG			: $\ddot{O}$ : - $\dot{N}$ = $\ddot{O}$ : $\rightarrow$ Cu @C-NG		
Atom type	$E_p$	Q	Atom type	$E_p$	Q	Atom type	$E_p$	Q
N1	-17.8974	0.0138	N1	-17.9023	0.0001	N1	-17.8793	0.0395
O2	-21.7065	-0.1115	O2	-21.7065	-0.1212	O2	-21.6890	-0.0991
O3	-21.9267	-0.1936	O3	-21.9372	-0.2173	O3	-21.9183	-0.1888
C9	-14.5480	-0.3492	C9	-14.5398	-0.4064	C9	-14.5414	-0.4128
C15	-14.4653	0.0591	C15	-14.4733	0.0599	C15	-14.4885	0.0551
C16	-14.4560	-0.2814	C16	-14.4737	-0.3711	C16	-14.4885	-0.3726
C17	-14.5684	-0.4658	C17	-14.6058	-0.5429	C17	-14.6196	-0.5217
Mn 18	-107.7744	1.5486	Co 18	-120.312	1.7938	Cu 18	-133.3453	1.7077
C19	-14.4372	0.0776	C19	-14.5038	-0.0058	C19	-14.4900	0.0091
C20	-14.6675	-0.0628	C20	-14.6703	-0.0463	C20	-14.6639	-0.0430
C24	-14.4956	-0.0711	C24	-14.5033	-0.0499	C24	-14.5126	-0.0561
C26	-14.4425	0.0725	C26	-14.4941	0.0094	C26	-14.5053	0.0468

In addition, in Figure3 (a-c), it has been plotted the electric potential of NQR method versus Mulliken charge for elements of : $\ddot{O}$ : - $\dot{N}$  =  $\ddot{O}$ :  $\rightarrow$  (Mn, Co, Cu)-doped nanographene using CAM-B3LYP/EPR-III, LANL2DZ, 6-31+G (d,p) level of theory.



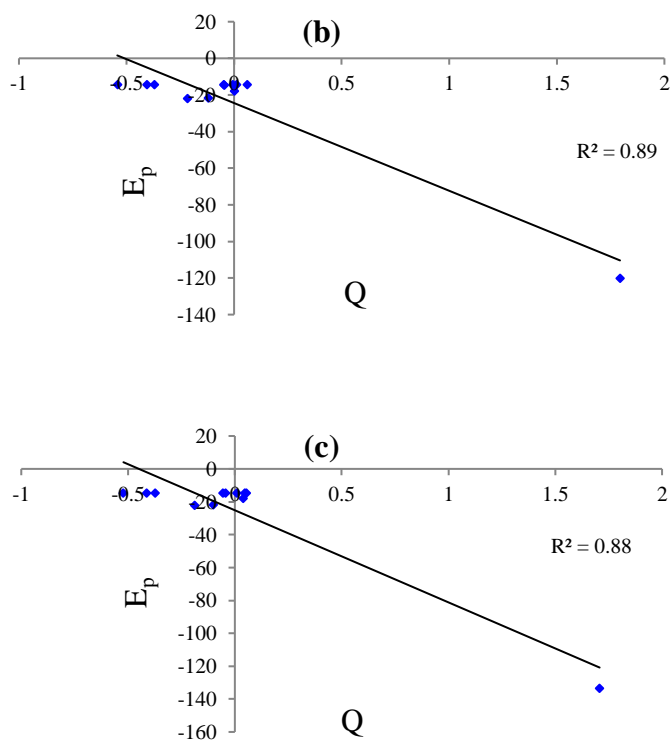


**Figure 3.** The electric potential versus Mulliken charge through NQR calculation for adsorption of NO<sub>2</sub> onto (a) Mn-, (b) Co-, (c) Cu-doped nanographene using CAM-B3LYP/EPR-III, LANL2DZ,6-31+G(d,p).

In Figure 3, the changes of electric potential for nitrogen, oxygen, carbon, manganese, cobalt, and copper in the active site of Langmuir adsorption have been remarked. In fact, it has been observed the effect of the substitution of carbon atoms in pristine graphene with manganese, cobalt, and copper during adsorbing NO<sub>2</sub> resulted in electric potential using NQR analysis (Figure3a-c). It's obvious that the graph  $:\ddot{O}:-\dot{N}=\ddot{O} \rightarrow \text{Mn}@ \text{C-NG}$ ,  $:\ddot{O}:-\dot{N}=\ddot{O} \rightarrow \text{Co}@ \text{C-NG}$ ,  $:\ddot{O}:-\dot{N}=\ddot{O} \rightarrow \text{Cu}@ \text{C-NG}$  fluctuated by Mn, Co, and Cu, respectively, which represent the efficiency of nitrogen dioxide detectors as promising scavengers.

### 3.3. Natural Bond Orbital (NBO) analysis.

Furthermore, the natural bond orbital (NBO) analysis [45] of NO<sub>2</sub> adsorption on the (Mn, Co, Cu) -doped carbon nanographene has illustrated the character of electronic conjugation between bonds in the gas molecules and TM@C-Gr (Table 2 & Figure 4).

**Table 2.** NBO analysis for adsorbing NO<sub>2</sub> on the (Mn, Co, Cu)@C-NG, respectively.

NO <sub>2</sub> → TM@C-Gr	Bond orbital	Occupancy	Hybrids
$:\ddot{O}:-\dot{N}=\ddot{O} \rightarrow \text{Mn}@ \text{C-NG}$	BD (1) N1 – O2	1.9482	0.6446 (sp <sup>3.94</sup> ) N + 0.7645 (sp <sup>4.00</sup> ) O
	BD (1) N1 – O3	1.9311	0.7591 (sp <sup>3.20</sup> ) N + 0.6509 (sp <sup>4.15</sup> ) O
	BD (1) C9 – Mn18	1.9329	0.7563 (sp <sup>1.75</sup> ) C + 0.6543 (sp <sup>0.20</sup> d <sup>4.96</sup> ) Mn
	BD (1) C16– Mn18	1.9103	0.8161 (sp <sup>1.69</sup> ) C + 0.5779 (sp <sup>0.80</sup> d <sup>2.09</sup> ) Mn
	BD (1) C17– Mn18	1.9496	0.7660 (sp <sup>1.55</sup> ) C + 0.6428 (sp <sup>0.33</sup> d <sup>4.15</sup> ) Mn
$:\ddot{O}:-\dot{N}=\ddot{O} \rightarrow \text{Co}@ \text{C-NG}$	BD (1) N1 – O2	1.9443	0.6399 (sp <sup>3.97</sup> ) N + 0.7684 (sp <sup>3.54</sup> ) O
	BD (1) N1 – O3	1.9248	0.7538 (sp <sup>3.17</sup> ) N + 0.6571 (sp <sup>3.69</sup> ) O
	BD (1) C9 – Co18	1.9641	0.8409 (sp <sup>1.29</sup> ) C + 0.5412 (sp <sup>0.88</sup> d <sup>2.85</sup> ) Co
	BD (1) C16– Co18	1.9557	0.8444 (sp <sup>1.50</sup> ) C + 0.5358 (sp <sup>1.14</sup> d <sup>2.04</sup> ) Co
	BD (1) C17– Co18	1.9734	0.8330 (sp <sup>1.30</sup> ) C + 0.5533 (sp <sup>0.79</sup> d <sup>4.09</sup> ) Co
$:\ddot{O}:-\dot{N}=\ddot{O} \rightarrow \text{Cu}@ \text{C-NG}$	BD (1) N1 – O2	1.9460	0.6398 (sp <sup>3.96</sup> ) N + 0.6398 (sp <sup>3.45</sup> ) O
	BD (1) N1 – O3	1.9220	0.7579 (sp <sup>3.16</sup> ) N + .6524 (sp <sup>3.60</sup> ) O
	BD (1) C9 – Cu18	1.9044	0.8390 (sp <sup>1.21</sup> ) C + 0.5442 (sp <sup>2.33</sup> d <sup>1.63</sup> ) Cu
	BD (1) C16– Cu18	1.9658	0.8422 (sp <sup>1.43</sup> ) C + 0.5392 (sp <sup>0.94</sup> d <sup>1.52</sup> ) Cu
	BD (1) C17– Cu18	1.9494	0.8390 (sp <sup>0.98</sup> ) C + 0.5442 (sp <sup>1.81</sup> d <sup>1.30</sup> ) Cu

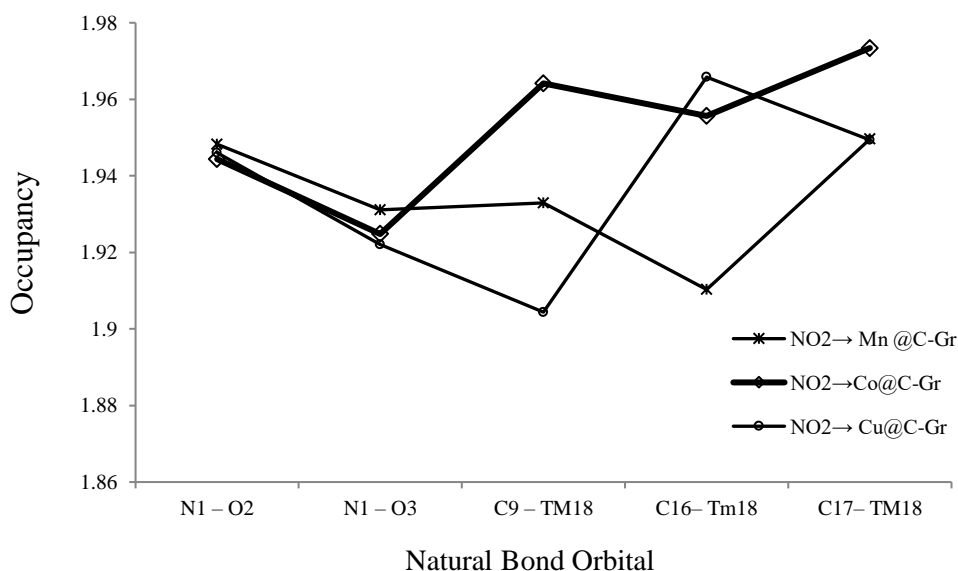


**Figure 4.** Occupancy fluctuation extracted of NBO method for bond lengths of N-O, N-TM (Mn, Co, Cu) through adsorption of NO<sub>2</sub> onto TM@C-Gr surface.

In Figure 4, the complexes of NO<sub>2</sub> → Mn@ C-NG, NO<sub>2</sub> → Co@ C-NG, NO<sub>2</sub> → Cu@ C-NG surfaces have exhibited the most fluctuated graphs through the occupancy via the natural bond orbitals due to the Langmuir adsorption while the active oxygen atoms in nitrogen dioxide becoming close to the nanographene.

### 3.4. Thermodynamic properties & IR spectroscopy analysis.

Thermodynamic parameters have been estimated for the adsorption of toxic nitrogen dioxide (: $\ddot{O}$ : - $\dot{N}$  =  $\ddot{O}$ :) on the surfaces of (Mn, Co, Cu), respectively, doping of nanographene as the gas sensors can be used as the selective detectors for environmentally hazardous gas (Table 3).

**Table 3.** The thermodynamic attributes of NO<sub>2</sub> adsorbed on the (Mn, Co, Cu)@C-Gr as the selective gas sensor.

Compound	$\Delta E^{\circ} \times 10^{-4}$ (kcal/mol)	$\Delta H^{\circ} \times 10^{-4}$ (kcal/mol)	$\Delta G^{\circ} \times 10^{-4}$ (kcal/mol)	$\Delta G^{\circ}_{ads} \times 10^{-4}$ (kcal/mol)	S <sup>o</sup> (Cal/K.mol)	Dipole moment (Debye)
: $\ddot{O}$ : - $\dot{N}$ = $\ddot{O}$ :	-12.6298	-12.6298	-12.6315	-	57.792	0.2323
Mn@ C-NG	-139.3551	-139.3551	-139.3588	-	124.779	1.4652
Co@ C-NG	-153.7094	-153.7094	-153.7133	-	128.964	0.9321
Cu@ C-NG	-169.6604	-169.6605	-169.6643	-	129.753	1.0422
: $\ddot{O}$ : - $\dot{N}$ = $\ddot{O}$ : → Mn @C-Gr	-151.9008	-151.9008	-151.9045	0.0858	125.163	10.5640
: $\ddot{O}$ : - $\dot{N}$ = $\ddot{O}$ : → Co @C-Gr	-166.2564	-166.2564	-166.2598	0.0850	116.087	4.6108
: $\ddot{O}$ : - $\dot{N}$ = $\ddot{O}$ : → Cu @C-Gr	-182.2074	-182.2073	-182.2110	0.0848	123.268	4.1641

Furthermore, the infrared spectrums for adsorption of NO<sub>2</sub> by (Mn, Co, Cu)-doped onto C-nanographene have been reported in Figure 5 (a-c).

The graphs have been observed in the frequency limitation of about 500 cm<sup>-1</sup>- 2000 cm<sup>-1</sup> for the complexes of : $\ddot{O}$ : - $\dot{N}$  =  $\ddot{O}$ : → Mn @C-NG, : $\ddot{O}$ : - $\dot{N}$  =  $\ddot{O}$ : → Co @ C-NG, and : $\ddot{O}$ : - $\dot{N}$  =  $\ddot{O}$ : → Cu @C-Gr with the strongest peaks in IR spectrum around 1550 cm<sup>-1</sup> and 1900 cm<sup>-1</sup> Figure5 (a-c) .



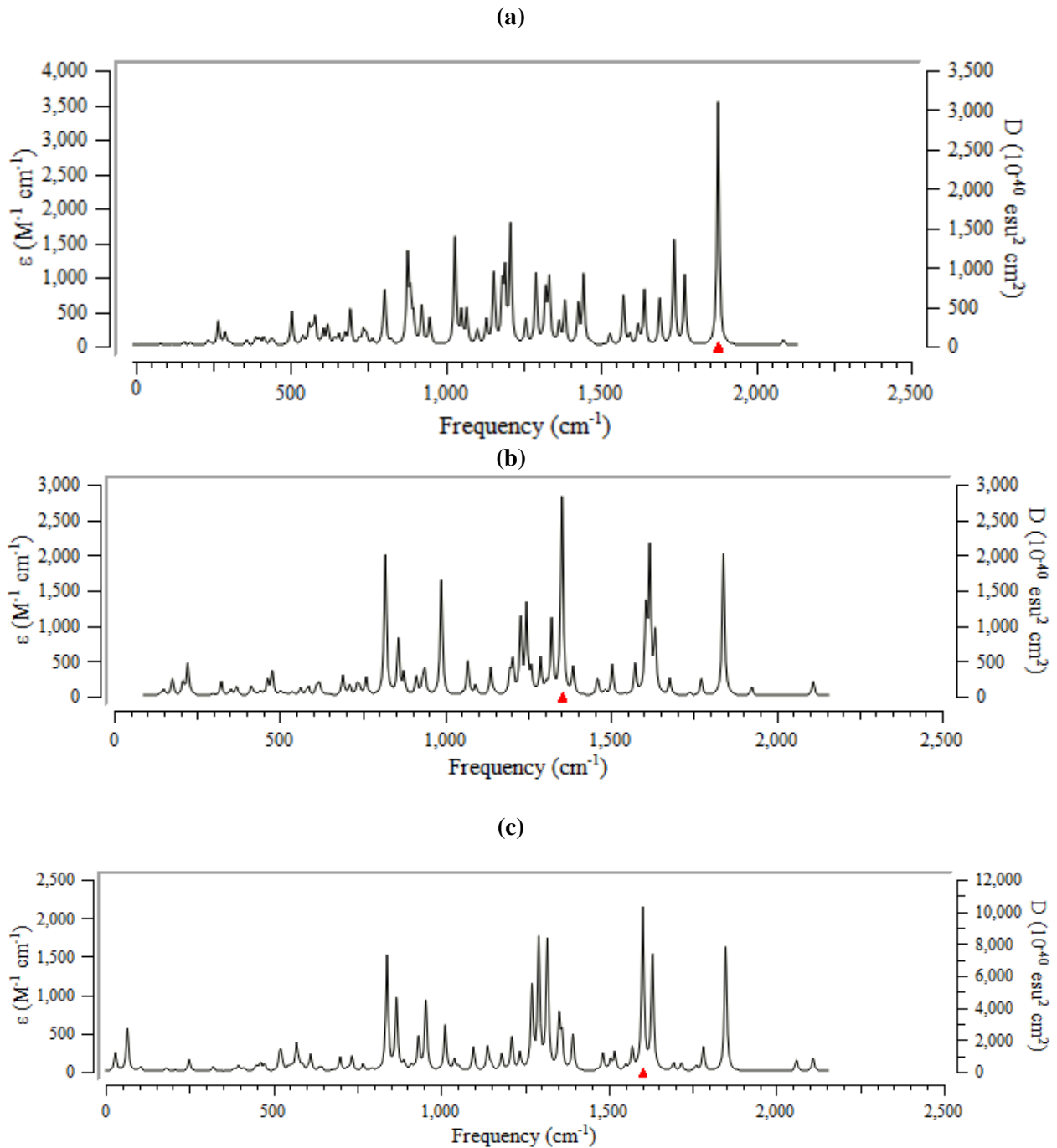


**Figure 5.** Alterations of frequency ( $\text{cm}^{-1}$ ) in the IR spectrums for (a)  $\ddot{\text{O}}: -\dot{\text{N}} = \ddot{\text{O}}: \rightarrow \text{Mn @C-NG}$ , (b)  $\ddot{\text{O}}: -\dot{\text{N}} = \ddot{\text{O}}: \rightarrow \text{Co @ C-NG}$ , (c)  $\ddot{\text{O}}: -\dot{\text{N}} = \ddot{\text{O}}: \rightarrow \text{Cu @C-NG}$  as the selective gas sensors.

From Figure 6, it could be understood that the maximum of the Langmuir adsorbing isotherm plots related to  $\Delta G_{\text{ads}}^0$  versus dipole moment may depend on the interactions between  $\text{NO}_2$  and TM-doped C-nanographene. The order of Gibbs free energy changes for clusters of gas  $\rightarrow \text{TM@ C-Gr}$  is  $\Delta G_{\text{NO}_2 \rightarrow \text{Mn@C}}^0 > \Delta G_{\text{NO}_2 \rightarrow \text{Co@C}}^0 > \Delta G_{\text{NO}_2 \rightarrow \text{Cu@C}}^0$ , respectively (Table3 & Figure 6).

The adsorptive capacity of  $\text{NO}_2$  on the TM-doped C-nanographene is approved by the  $\Delta G_{\text{ads}}^0$  amounts:

$$\Delta G_{\text{ads,NO}_2}^0 = \Delta G_{\text{NO}_2 \rightarrow \text{TM@C-Gr}}^0 - (\Delta G_{\text{NO}_2}^0 + \Delta G_{\text{TM@C-Gr}}^0); \quad (\text{TM} = \text{Mn, Co, Cu}) \quad (6)$$

On the basis of the data in Table 3, it is predicted that the adsorption of NO<sub>2</sub> on the TM-doped graphene nanosheet must be physicochemical attributes. As seen in Figure 6, all the calculated  $\Delta G_{ads,NO_2}^0$  values are very similar, which exhibits the accord of the estimated data by all approaches and the accuracy of the measurements. In fact, TM-doped C-nanographene can possess enough efficiency for the adsorption of toxic gas of nitrogen dioxide through charge transfer from oxygen atoms to transition metals.

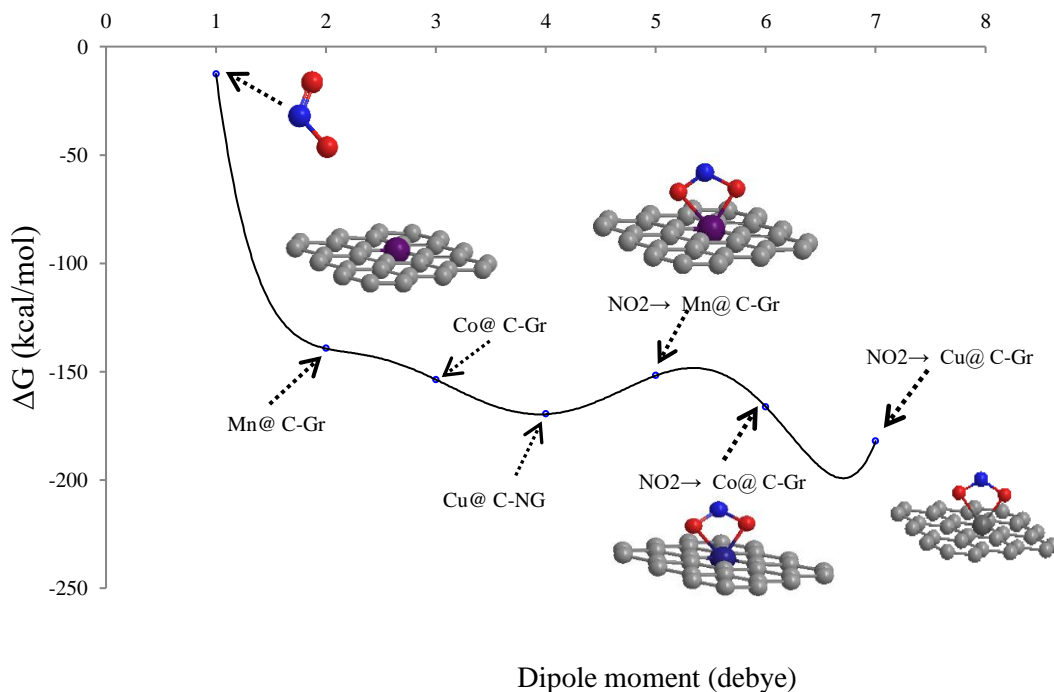


**Figure 6.** The changes of Gibbs free energy (kcal/mol) versus dipole moment (Debye) for adsorption of NO<sub>2</sub> on the (Mn, Co, Cu), respectively, doping of C-nanographene surface.

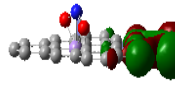
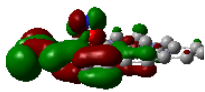
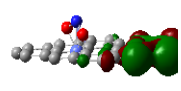
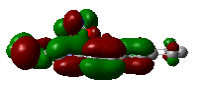
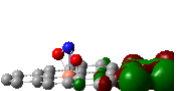
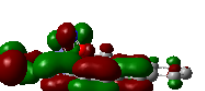
### 3.5. Frontier molecular orbital's of HOMO, LUMO, and UV-VIS analysis.

The lowest unoccupied molecular orbital (LUMO) energy is generated by ionization, and the highest occupied molecular orbital (HOMO) energy is observed by the electron affinity. These parameters have been evaluated for the adsorption of nitrogen dioxide on the (Mn, Co, Cu) doping of nanographene as the gas detector in Table 4. The HOMO (au), LUMO (au), and band energy gap ( $\Delta E = E_{LUMO} - E_{HOMO}$ ) (eV) have exhibited the pictorial explanation of the frontier molecular orbital's and their respective positive and negative areas, which are a significant parameter for discovering the molecular properties of efficient compounds in adsorption of NO<sub>2</sub> on the TM-doped nanographene surface (Table 4).

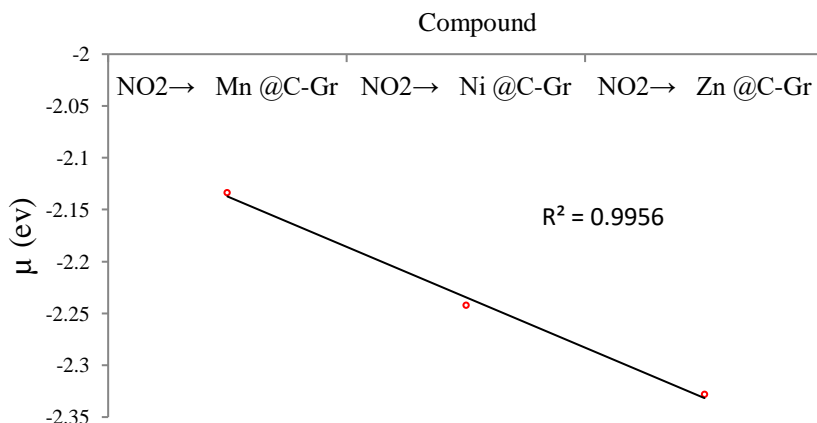
Moreover, for getting more conclusive approval in identifying the compound characteristics of adsorption complexes of NO<sub>2</sub> on the (Mn, Co, Cu) doping of C-nanographene surfaces, a series of chemical reactivity parameters such as chemical potential ( $\mu$ ), electronegativity ( $\chi$ ), hardness ( $\eta$ ), softness ( $\zeta$ ), electrophilicity index ( $\psi$ ) has been carried out (Table 4) [46-51].

Figure 7 has drawn that chemical potential ( $\mu$ ) for NO<sub>2</sub> adsorption on the surface of zinc doping of carbon-nanographene has a considerable minimum potential well. The negative content of the chemical potential ( $\mu$ ) and the positive contents of other factors have remarked an admissible efficiency of scavenging NO<sub>2</sub> by zinc-doped carbon-nanographene. In fact, the chemical potential defined the increase of NO<sub>2</sub> molecules to the crystal of Zn@ C-Gr while the number of other particles and the number of unoccupied lattice locations remain constant.

**Table 4.** The LUMO (a.u.), HOMO (a.u.), band energy gap ( $\Delta E$  /eV), and other qualifications (eV) for adsorption of NO<sub>2</sub> on the (Mn, Co, Cu) doping of C-nanographene surfaces using CAM-B3LYP/ LANL2DZ, 6-31+G (d, p).

Gas→ TM@C-NG	LUMO	HOMO	$\Delta E$	$\mu$	$\chi$	$\eta$	$\zeta$	$\psi$
: $\ddot{O}$ : - $\dot{N}$ = $\ddot{O}$ : → Mn@ C-NG	 -0.0088	 -0.1479	3.7853	-2.1335	2.1335	1.8927	0.2641	1.2024
: $\ddot{O}$ : - $\dot{N}$ = $\ddot{O}$ : → Co@ C-NG	 -0.0077	 -0.1570	4.0621	-2.2419	2.2419	2.0310	0.2462	1.2373
: $\ddot{O}$ : - $\dot{N}$ = $\ddot{O}$ : → Cu@ C-NG	 -0.0115	 -0.1596	4.0302	-2.3280	2.3280	2.0151	0.2481	1.3447

$\Delta E = E_{LUMO} - E_{HOMO}$ ;  $\mu = (E_{HOMO} + E_{LUMO})/2$ ;  $\chi = -(E_{HOMO} + E_{LUMO})/2$ ;  $\eta = (E_{LUMO} - E_{HOMO})/2$ ;  $\zeta = 1/(2\eta)$ ;  $\psi = \mu^2/(2\eta)$



**Figure 7.** The chemical potential ( $\mu$ ) of NO<sub>2</sub> adsorption onto the crystal of Zn@C-Gr.

As a matter of fact, enhancement of the gas molecules of NO<sub>2</sub> thus involves simultaneously increasing a lattice site or unit cell to the crystal of Zn@ C-Gr surface. This procedure leads to an increase in the surface region, and thereby, energy must be spent generating a new nanographene surface [52-59]. In addition, the alliance of particles alters the mass of the crystal, and the process is also accomplished versus the mechanical powers.

In this work, the energy gap establishes how toxic gas of NO<sub>2</sub> can be adsorbed on the (Mn, Co, Cu) doping of nanographene as the gas sensors at B3LYP/ LANL2DZ, 6-311+G (d, p) quantum approach. In addition, frontier molecular orbitals perform an essential function in optical and electrical factors like ultraviolet and visible spectrums [60-69].

The energy gap between LUMO and HOMO has recognized the qualifications of molecular electrical transport [50]. Through the Frank-Condon formula, the highest absorption peak value (max) is related to an ultraviolet and visible spectrum to vertical stimulation.

## 4. Conclusions

This research aimed to remark on the study of polluting gas of nitrogen dioxide adsorption employing graphene nanosheet. The graphene sheet reviewed, in general, physically adsorbs many of the pollutant gas molecules considered, and the interaction can usually be enhanced by transition metal doping, which ameliorates their detecting properties through chemisorption study.

This article has reported the trends for environmental pollutant gas of nitrogen dioxide (NO<sub>2</sub>) chemisorption on transition metals (manganese, cobalt, copper) doping of carbon-nanographene surface.

In particular, the energetic, structural, and infrared adsorption characteristics of linearly (atop) NO<sub>2</sub> adsorbed on (Mn, Co, Cu) doping of C-NG have been discussed. Spin-unrestricted density functional theory (DFT) calculations were applied to verdict the tendency of NO<sub>2</sub> adsorption energy of (NO<sub>2</sub>→ Mn-, NO<sub>2</sub>→Co-, NO<sub>2</sub>→Cu-) doped on the nanographene sheet and normal mode vibrational frequencies ( $\nu_{\text{NO}_2}$ ) of:  $\ddot{\text{O}}: -\dot{\text{N}} = \ddot{\text{O}}:$  for clusters composed of Mn, Co, Cu.

The effects of the transition metal electronic structure on the adsorption energy of toxic NO<sub>2</sub> gas and how these chemical factors might be related to the catalytic activity of transition-supported metal catalysts that deal with adsorption and surface diffusion have been investigated.

## Acknowledgments

In successfully completing this paper and its research, the authors are grateful to Kastamonu University for their support through the library, the laboratory, and scientific websites.

## Conflicts of Interest

The authors declare no conflict of interest.

## References

1. Kumar, R.; Jaiswal, M.; Kushwaha, N.; Bansal, S.; Mazumder, N.; Mittal, J. Nanomaterial-Based Gas Sensors for Agriculture Sector. In: Pudake, R.N., Jain, U., Kole, C. (eds) Biosensors in Agriculture: Recent Trends and Future Perspectives. Concepts and Strategies in Plant Sciences. *Springer, Cham*. **2021**, [https://doi.org/10.1007/978-3-030-66165-6\\_4](https://doi.org/10.1007/978-3-030-66165-6_4).
2. Liu, J. Mapping high resolution national daily NO<sub>2</sub> exposure across mainland China using an ensemble algorithm. *Environ. Pollut.* **2021**, *279*, 116932. <https://doi.org/10.1016/j.envpol.2021.116932>.
3. Akhter, F.; Alahi, M.E.E.; Siddiquei, H.R.; Gooneratne, C.P.; Mukhopadhyay, S.C. Graphene oxide (GO) coated impedimetric gas sensor for selective detection of carbon dioxide (CO<sub>2</sub>) with temperature and humidity compensation. *IEEE Sens. J.* **2021**, *21*, 4241–4249. <https://doi.org/10.1109/JSEN.2020.3035795>.
4. Despot, D.; Pacheco Fernández, M.; Barjenbruch, M. Comparison of Online Sensors for Liquid Phase Hydrogen Sulphide Monitoring in Sewer Systems. *Water* **2021**, *13*, 1876. <https://doi.org/10.3390/w13131876>.
5. Kumar, N.; Gupta, H. Chapter 18—Methane: Risk assessment, environmental, and health hazard. In *Hazardous Gases, Risk Assessment on the Environment and Human Health*; Academic Press: Cambridge, MA, USA, **2021**, 225–238. <https://doi.org/10.1016/B978-0-323-89857-7.00009-8>.
6. Fernández, M.P.; Despot, D.; Barjenbruch, M. Comparison of H<sub>2</sub>S Gas Sensors: A Sensor Management Procedure for Sewer Monitoring. *Sustainability* **2021**, *13*, 10779. <https://doi.org/10.3390/su131910779>.
7. Mishra, S.K.; Verma, R.K.; Mishra, A.K. Versatile Sensing Structure: GaP/Au/Graphene/Silicon. *Photonics* **2021**, *8*, 547. <https://doi.org/10.3390/photonics8120547>.

8. Dong, Q.; Xiao, M.; Chu, Z.; Li, G.; Zhang, Y. Recent Progress of Toxic Gas Sensors Based on 3D Graphene Frameworks. *Sensors* **2021**, *21*, 3386. <https://doi.org/10.3390/s21103386>.
9. Mishra, S.K.; Mishra, A.K. ITO/Polymer matrix assisted surface plasmon resonance based fiber optic sensor. *Results Opt.* **2021**, *5*, 100173. <https://doi.org/10.1016/j.rio.2021.100173>.
10. Liu, K.; Zhang, R.; Liu, Y.; Chen, X.; Li, K.; Pickwell-Macpherson, E. Gold nanoparticle enhanced detection of EGFR with a terahertz metamaterial biosensor. *Biomed. Opt. Express* **2021**, *12*, 1559–1567. <https://doi.org/10.1364/BOE.418859>.
11. Monajjemi, M.; Khaleghian, M.; Tadayonpour, N.; Mollaamin, F. The effect of different solvents and temperatures on stability of single-walled carbon nanotube: A QM/MD study, *Int. J. Nanosci.* **2010**, *09*, 517–529. <https://doi.org/10.1142/S0219581X10007071>.
12. Mollaamin, F.; Monajjemi, M. Graphene Embedded with Transition Metals for Capturing Carbon Dioxide: Gas Detection Study Using QM Methods. *Clean Technol.* **2023**, *5*, 403–417. <https://doi.org/10.3390/cleantechnol5010020>.
13. Mollaamin, F.; Monajjemi, M. Doping of Graphene Nanostructure with Iron, Nickel and Zinc as Selective Detector for the Toxic Gas Removal: A Density Functional Theory Study. *C* **2023**, *9*, 20. <https://doi.org/10.3390/c9010020>.
14. Arroyo, P.; Gómez-Suárez, J.; Suárez, J.I.; Lozano, J. Low-Cost Air Quality Measurement System Based on Electrochemical and PM Sensors with Cloud Connection. *Sensors* **2021**, *21*, 6228. <https://doi.org/10.3390/s21186228>.
15. Neubert, S.; Roddelkopf, T.; Al-Okby, M.F.R.; Junginger, S.; Thurow, K. Flexible IoT Gas Sensor Node for Automated Life Science Environments Using Stationary and Mobile Robots. *Sensors* **2021**, *21*, 7347. <https://doi.org/10.3390/s21217347>.
16. Zhou, T.; Zhang, T. Recent Progress of Nanostructured Sensing Materials from 0D to 3D: Overview of Structure–Property–Application Relationship for Gas Sensors. *Small Methods* **2021**, *5*, 2100515. <https://doi.org/10.1002/smt.202100515>.
17. Yoon, B.; Choi, S.-J.; Swager, T.M.; Walsh, G.F. Flexible Chemiresistive Cyclohexanone Sensors Based on Single-Walled Carbon Nanotube–Polymer Composites. *ACS Sens.* **2021**, *6*, 3056–3062. <https://doi.org/10.1021/acssensors.1c01076>.
18. Bezdek, M.J.; Luo, S.X.L.; Liu, R.Y.; He, Q.; Swager, T.M. Trace Hydrogen Sulfide Sensing Inspired by Polyoxometalate-Mediated Aerobic Oxidation. *ACS Cent. Sci.* **2021**, *7*, 1572–1580. <https://doi.org/10.1021/acscentsci.1c00746>.
19. Inaba, M.; Oda, T.; Kono, M.; Phansiri, N.; Morita, T.; Nakahara, S.; Nakano, M.; Suehiro, J. Effect of mixing ratio on NO<sub>2</sub> gas sensor response with SnO<sub>2</sub>-decorated carbon nanotube channels fabricated by one-step dielectrophoretic assembly. *Sens. Actuators B* **2021**, *344*, 130257. <https://doi.org/10.1016/j.snb.2021.130257>.
20. Ramirez-de-Arellano, J.M.; Canales, M.; Magaña, L.F. Carbon Nanostructures Doped with Transition Metals for Pollutant Gas Adsorption Systems. *Molecules* **2021**, *26*, 5346. <https://doi.org/10.3390/molecules26175346>.
21. Schultealbert, C.; Amann, J.; Baur, T.; Schütze, A. Measuring Hydrogen in Indoor Air with a Selective Metal Oxide Semiconductor Sensor. *Atmosphere* **2021**, *12*, 366. <https://doi.org/10.3390/atmos12030366>.
22. Liu, H.; Meng, G.; Deng, Z.; Nagashima, K.; Wang, S.; Dai, T.; Li, L.; Yanagida, T.; Fang, X. Discriminating BTX Molecules by the Nonselective Metal Oxide Sensor-Based Smart Sensing System. *ACS Sens.* **2021**, *6*, 4167–4175. <https://doi.org/10.1021/acssensors.1c01704>.
23. Krivetskiy, V.V.; Andreev, M.D.; Efitorov, A.O.; Gaskov, A.M. Statistical shape analysis pre-processing of temperature modulated metal oxide gas sensor response for machine learning improved selectivity of gases detection in real atmospheric conditions. *Sens. Actuators B Chem.* **2021**, *329*, 129187. <https://doi.org/10.1016/j.snb.2020.129187>.
24. Bakhshi, K.; Mollaamin, F.; Monajjemi, M. Exchange and correlation effect of hydrogen chemisorption on nano V(100) surface: A DFT study by generalized gradient approximation (GGA). *J. Comput. Theor. Nanosci.* **2011**, *8*, 763–768. <https://doi.org/10.1166/jctn.2011.1750>
25. Mollaamin, F.; Monajjemi, M.; Salemi, S.; Baei, M.T. A Dielectric Effect on Normal Mode Analysis and Symmetry of BNNT Nanotube. *Fuller. Nanotub. Carbon Nanostructures* **2011**, *19*, 182–196. <https://doi.org/10.1080/15363831003782932>.

26. Monajjemi, M.; Baie, M.T.; Mollaamin, F. Interaction between threonine and cadmium cation in [Cd(Thr)] (n = 1-3) complexes: Density functional calculations , *Russian Chemical Bulletin*, **2010**, *59*, 886-889. <https://doi.org/10.1007/s11172-010-0181-5>.
27. Zadeh, M. A. A.; Lari, H.; Kharghanian, L.; Balali, E.; Khadivi, R.; Yahyaei, H.; Mollaamin, F.; Monajjemi, M. Density functional theory study and anti-cancer properties of shyshaq plant: In view point of nano biotechnology, *Journal of Computational and Theoretical Nanoscience*, **2015**, *12*, 4358-4367. <https://doi.org/10.1166/jctn.2015.4366>.
28. Noh, J.; Kwon, S.-H.; Park, S.; Kim, K.-K.; Yoon, Y.-J. TiO<sub>2</sub> Nanorods and Pt Nanoparticles under a UV-LED for an NO<sub>2</sub> Gas Sensor at Room Temperature. *Sensors* **2021**, *21*, 1826. <https://doi.org/10.3390/s21051826>.
29. Mollaamin, F.; Ilkhani, A.; Sakhaei, N.; Bonsakhteh, B.; Faridchehr, A.; Tohidi, S.; Monajjemi, M. Thermodynamic and solvent effect on dynamic structures of nano bilayer-cell membrane: Hydrogen bonding study, *Journal of Computational and Theoretical Nanoscience*, **2015**, *12*, 3148-3154. <https://doi.org/10.1166/jctn.2015.4092>.
30. Jayaprakash, G.K. Pre-post redox electron transfer regioselectivity at the alanine modified nano graphene electrode interface. *Chem. Phys. Lett.* **2021**, *789*, 139295. <https://doi.org/10.1016/j.cplett.2021.139295>.
31. Makarova, E.S.; Novotelnova, A.V. Estimating the uncertainty of measurements of thermal conductivity of thin films of thermoelectrics with the 3-omega method. *J. Phys. Conf. Ser.* **2021**, *2057*, 012108. <https://doi.org/10.1088/1742-6596/2057/1/012108>.
32. Mollaamin, F. & Monajjemi, M. Molecular modelling framework of metal-organic clusters for conserving surfaces: Langmuir sorption through the TD-DFT/ONIOM approach. *MOLECULAR SIMULATION*, **2023**, *49*, 365-376. <https://doi.org/10.1080/08927022.2022.2159996>.
33. Svensson, M.; Humbel, S.; Froese, R.D.J.; Matsubara, T.; Sieber, S.; and Morokuma, K. ONIOM: A Multilayered Integrated MO + MM Method for Geometry Optimizations and Single Point Energy Predictions. A Test for Diels–Alder Reactions and Pt(P(t-Bu)<sub>3</sub>)<sub>2</sub> + H<sub>2</sub> Oxidative Addition. *J. Phys. Chem.* **1996**, *100*, 19357–19363. <https://doi.org/10.1021/jp962071j>.
34. Mollaamin, F.; Shahriari, S.; Monajjemi, M. et al. Nanocluster of Aluminum Lattice via Organic Inhibitors Coating: A Study of Freundlich Adsorption. *J. Clust. Sci.* **2023**, *34*, 1547–1562. <https://doi.org/10.1007/s10876-022-02335-1>.
35. Felix Brandt, Christoph R. Jacob. Systematic QM Region Construction in QM/MM Calculations Based on Uncertainty Quantification. *Journal of Chemical Theory and Computation* **2022**, *18*, 2584-2596. <https://doi.org/10.1021/acs.jctc.1c01093>.
36. Becke, A.D. Density-functional thermochemistry. III. The role of exact exchange. *J. Chem. Phys.* **1993**, *98*, 5648–5652. <https://doi.org/10.1063/1.464913>.
37. Lee, C.; Yang, W.; Parr, R.G. Development of the Colle–Salvetti correlation-energy formula into a functional of the electron density. *Phys. Rev. B* **1988**, *37*, 785–789. <https://doi.org/10.1103/PhysRevB.37.785>.
38. Becke, A.D. Density-functional exchange-energy approximation with correct asymptotic behavior. *Phys. Rev. A* **1988**, *38*, 3098–3100. <https://doi.org/10.1103/PhysRevA.38.3098>.
39. Ditchfield, R.; Hehre, W.J.; Pople, J.A. Self-consistent molecular-orbital methods. IX. An extended Gaussian-type basis for molecular-orbital studies of organic molecules. *J. Chem. Phys.* **1971**, *54*, 724–728. <https://doi.org/10.1063/1.1674902>.
40. Frisch, M. J.; Trucks, G. W.; Schlegel, H. B.; Scuseria, G. E.; Robb, M. A.; Cheeseman, J. R.; Scalmani, G.; Barone, V.; Petersson, G. A.; Nakatsuji, H.; Li, X.; Caricato, M.; Marenich, A. V.; Bloino, J.; Janesko, B. G.; Gomperts, R.; Mennucci, B.; Hratchian, H. P.; Ortiz, J. V.; Izmaylov, A. F.; Sonnenberg, J. L.; Williams-Young, D.; Ding, F.; Lipparini, F.; Egidi, F.; Goings, J.; Peng, B.; Petrone, A.; Henderson, T.; Ranasinghe, D.; Zakrzewski, V. G.; Gao, J.; Rega, N.; Zheng, G.; Liang, W.; Hada, M.; Ehara, M.; Toyota, K.; Fukuda, R.; Hasegawa, J.; Ishida, M.; Nakajima, T.; Honda, Y.; Kitao, O.; Nakai, H.; Vreven, T.; Throssell, K.; Montgomery, J. A., Jr.; Peralta, J. E.; Ogliaro, F.; Bearpark, M. J.; Heyd, J. J.; Brothers, E. N.; Kudin, K. N.; Staroverov, V. N.; Keith, T. A.; Kobayashi, R.; Normand, J.; Raghavachari, K.; Rendell, A. P.; Burant, J. C.; Iyengar, S. S.; Tomasi, J.; Cossi, M.; Millam, J. M.; Klene, M.; Adamo, C.; Cammi, R.; Ochterski, J. W.; Martin, R. L.; Morokuma, K.; Farkas, O.; Foresman, J. B.; Fox, D. J. Gaussian 16, Revision C.01, Gaussian, Inc., Wallingford CT, **2016**, <https://gaussian.com/citation/>.
41. Mollaamin, F. & Monajjemi, M. Electric and Magnetic Evaluation of Aluminum–Magnesium Nanoalloy Decorated with Germanium Through Heterocyclic Carbenes Adsorption: A Density Functional Theory Study. *Russ. J. Phys. Chem. B* **2023**, *17*, 658–672.

42. Mollaamin, F. & Monajjemi, M. In Silico-DFT Investigation of Nanocluster Alloys of Al-(Mg, Ge, Sn) Coated by Nitrogen Heterocyclic Carbenes as Corrosion Inhibitors. *J Clust Sci.* **2023**. <https://doi.org/10.1007/s10876-023-02436-5>.
43. Mollaamin, F. & Monajjemi, M. Tailoring and functionalizing the graphitic-like GaN and GaP nanostructures as selective sensors for NO, NO<sub>2</sub>, and NH<sub>3</sub> adsorbing: a DFT study. *J Mol Model* **2023**, *29*, 170. <https://doi.org/10.1007/s00894-023-05567-8>.
44. Mollaamin, F. & Monajjemi, M. Transition metal (X = Mn, Fe, Co, Ni, Cu, Zn)-doped graphene as gas sensor for CO<sub>2</sub> and NO<sub>2</sub> detection: a molecular modeling framework by DFT perspective. *J Mol Model* **2023**, *29*, 119. <https://doi.org/10.1007/s00894-023-05526-3>.
45. Tahan, A.; Mollaamin, F.; Monajjemi, M. Thermochemistry and NBO analysis of peptide bond: Investigation of basis sets and binding energy. *Russian Journal of Physical Chemistry A* **2009**, *83*, 587-597. <https://doi.org/10.1134/S003602440904013X>.
46. Kohn, W.; Becke, A.D.; Parr, R.G. Density Functional Theory of Electronic Structure. *J. Phys. Chem.* **1996**, *100*, 12974–12980. <https://doi.org/10.1021/jp960669l>.
47. Parr, R.G. and Pearson, R.G. Absolute Hardness: Companion Parameter to Absolute Electronegativity. *J. Am. Chem. Soc.* **1983**, *105*, 7512-7516. <http://dx.doi.org/10.1021/ja00364a005>.
48. Mollaamin, F. & Monajjemi, M. Tribocorrosion Framework of (Iron, Nickel, Zinc)-Doped Graphene Nanosheet: New Sights into Sulfur Dioxide and Hydrogen Sulfide Removal Using DFT/TD-DFT Methods. *J Bio Tribo Corros* **2023**, *9*, 47. <https://doi.org/10.1007/s40735-023-00768-3>.
49. Mollaamin, F. & Monajjemi, M. Corrosion Inhibiting by Some Organic Heterocyclic Inhibitors Through Langmuir Adsorption Mechanism on the Al-X (X = Mg/Ga/Si) Alloy Surface: A Study of Quantum Three-Layer Method of CAM-DFT/ONIOM. *J Bio Tribo Corros* **2023**, *9*, 33. <https://doi.org/10.1007/s40735-023-00751-y>.
50. Khalili Hadad, B.; Mollaamin, F.; Monajjemi, M. Biophysical chemistry of macrocycles for drug delivery: A theoretical study, *Russian Chemical Bulletin*, **2011**, *60*, 238-241. <https://doi.org/10.1007/s11172-011-0039-5>.
51. Mollaamin, F.; Monajjemi, M. Harmonic Linear Combination and Normal Mode Analysis of Semiconductor Nanotubes Vibrations. *J. Comput. Theor. Nanosci* **2015**, *12*, 1030-1039. <https://doi.org/10.1166/jctn.2015.3846>.
52. Monajjemi, M.; Mahdavian, L.; Mollaamin, F.; Khaleghian, M. Interaction of Na, Mg, Al, Si with carbon nanotube (CNT): NMR and IR study. *Russ. J. Inorg. Chem* **2009**, *54*, 1465-1473. <https://doi.org/10.1134/S0036023609090216>.
53. Khaleghian, M.; Zahmatkesh, M.; Mollaamin, F.; Monajjemi, M. Investigation of Solvent Effects on Armchair Single-Walled Carbon Nanotubes: A QM/MD Study. *Fuller. Nanotub. Carbon Nanostructures*. **2011**, *19*, 251-261, <https://doi.org/10.1080/15363831003721757>.
54. Mollaamin, F. & Monajjemi, M. Application of DFT and TD-DFT on Langmuir Adsorption of Nitrogen and Sulfur Heterocycle Dopants on an Aluminum Surface Decorated with Magnesium and Silicon. *Computation*. **2023**, *11*(6):108. <https://doi.org/10.3390/computation11060108>.
55. Sarasia, E.M.; Afsharnezhad, S.; Honarparvar, B.; Mollaamin, F.; Monajjemi, M. Theoretical study of solvent effect on NMR shielding tensors of luciferin derivatives. *Phys Chem Liquids* **2011**, *49*, 561-571, <https://doi.org/10.1080/00319101003698992>.
56. Monajjemi, M.; Mollaamin, F.; Gholami, M.R.; Yoosbashizadeh, H.; Sadrnezhad, S.K.; Passdar, H. Quantum Chemical Parameters of Some Organic Corrosion Inhibitors, Pyridine, 2-Picoline 4-Picoline and 2,4-Lutidine, Adsorption at Aluminum Surface in Hydrochloric and Nitric Acids and Comparison Between Two Acidic Media. *Main Group Met. Chem.* **2003**, *26*, 349-362, <https://doi.org/10.1515/MGMC.2003.26.6.349>.
57. Ghalandari, B.; Monajjemi, M.; Mollaamin, F. Theoretical Investigation of Carbon Nanotube Binding to DNA in View of Drug Delivery. *J. Comput. Theor. Nanosci* **2011**, *8*, 1212-1219, <https://doi.org/10.1166/jctn.2011.1801>.
58. Monajjemi, M.; Baheri, H.; Mollaamin, F. A percolation model for carbon nanotube-polymer composites using the Mandelbrot-Given. *Journal of Structural Chemistry* **2011**, *52*, 54-59, <https://doi.org/10.1134/S0022476611010070>.
59. Monajjemi, M.; Noei, M.; Mollaamin, F. Design of fMet-tRNA and Calculation of its Bonding Properties by Quantum Mechanics. *Nucleosides, Nucleotides & Nucleic Acids*. **2010**, *29* (9), 676-683. <https://doi.org/10.1080/15257771003781642>.
60. Monajjemi, M. Liquid-phase exfoliation (LPE) of graphite towards graphene: An ab initio study. *Journal of Molecular Liquids* **2017**, *230*, 461–472, <https://doi.org/10.1016/j.molliq.2017.01.044>.

61. Mahdavian, L.; Monajjemi, M. Alcohol sensors based on SWNT as chemical sensors: Monte Carlo and Langevin dynamics simulation. *Microelectronics journal* **2010**, *41*, 142-149, <https://doi.org/10.1016/j.mejo.2010.01.011>.
62. Monajjemi, M.; Boggs, J.E. A New Generation of BnNn Rings as a Supplement to Boron Nitride Tubes and Cages. *J. Phys. Chem. A* **2013**, *117*, 1670-1684, <http://dx.doi.org/10.1021/jp312073q>.
63. Monajjemi, M. Non bonded interaction between BnNn (stator) and BN B (rotor) systems: A quantum rotation in IR region. *Chemical Physics* **2013**, *425*, 29-45, <https://doi.org/10.1016/j.chemphys.2013.07.014>.
64. Monajjemi, M. Quantum investigation of non-bonded interaction between the B15N15 ring and BH2NBH2 (radical, cation, and anion) systems: a nano molecular motor. *Struct Chem* **2012**, *23*, 551-580, <http://dx.doi.org/10.1007/s11224-011-9895-8>.
65. Monajjemi, M. Metal-doped graphene layers composed with boron nitride-graphene as an insulator: a nanocapacitor. *Journal of Molecular Modeling* **2014**, *20*, 2507, <https://doi.org/10.1007/s00894-014-2507-y>.
66. Monajjemi, M.; Robert, W.J.; Boggs, J.E. NMR contour maps as a new parameter of carboxyl's OH groups in amino acids recognition: A reason of tRNA-amino acid conjugation. *Chemical Physics* **2014**, *433*, 1-11, <https://doi.org/10.1016/j.chemphys.2014.01.017>.
67. Monajjemi, M. Cell membrane causes the lipid bilayers to behave as variable capacitors: A resonance with self-induction of helical proteins. *Biophysical Chemistry* **2015**, *207*, 114-127, <https://doi.org/10.1016/j.bpc.2015.10.003>.
68. Monajjemi, M.; Bagheri, S.; Moosavi, M.S. *et al.* Symmetry breaking of B2N(-,0,+): An aspect of the electric potential and atomic charges. *Molecules* **2015**, *20*, 21636-21657, <https://doi.org/10.3390/molecules201219769>.
69. Mollaamin, F. & Monajjemi, M. Graphene-based resistant sensor decorated with Mn, Co, Cu for nitric oxide detection: Langmuir adsorption & DFT method. *Sensor Review*, **2023**. <https://doi.org/10.1108/SR-03-2023-0040>.